

A MODEL BASED IDENTIFICATION METHOD OF TRANSVERSE CRACKS IN ROTATING SHAFTS SUITABLE FOR INDUSTRIAL MACHINES

PAOLO PENNACCHI, NICOLÒ BACHSCHMID, ANDREA VANIA

*Dipartimento Di Meccanica,
Politecnico di Milano,
Via La Masa 34, I-20156 Milano
paolo.pennacchi@polimi.it, nicolo.bachschmid@polimi.it, andrea.vania@polimi.it*

Please send proofs to
*PROF. PAOLO PENNACCHI
Dipartimento di Meccanica,
Politecnico di Milano,
Via La Masa 34, I-20156 Milano*

ABSTRACT

This paper presents a model based transverse crack identification method suitable for industrial machines. The method is validated by experimental results obtained on a large test rig, which was expressly designed for investigating the dynamical behaviour of cracked horizontal rotors. The identification method and the relative theory is briefly presented, while three different types of crack are considered: the first is a slot, therefore not actually a crack since it has not the typical breathing behaviour, the second a small crack (14% of the diameter) and the third a deep crack (47% of the diameter). The excellent accuracy obtained in identifying position and depth of different cracks proves the effectiveness and reliability of the proposed method.

Keywords: *Rotor dynamics; Crack; Identification; Crack depth; Crack position.*

1 INTRODUCTION

Early papers documenting crack occurrences in real machines date back to the end of '60s and to '70s [1]-[4]. Propagating transverse cracks have been discovered in the last 20 years [5]-[6] in several rotors of steam turbines or generators of European power plants. Fortunately, as far as the authors know, they have been detected before the crack had propagated to a critical depth, that means before the occurrence of a catastrophic failure.

The importance of early detection of cracks, possibly by means of an automatic diagnostic methodology that uses the information furnished by standard monitoring systems, which generally analyze the vibrations measured in correspondence of the bearings only, appears obvious from these considerations.

Many different publications deal with the problem of crack identification in rotating shafts [7]-[11], but the methods seem to be unsuitable for application to real machines in operating conditions and have never been tested nor validated with experimental results.

In Imam's et al. paper [7], the effect of the presence of a crack is emphasized by huge bending loads and the crack detection is validated by means of laboratory tests and measurements, which are inapplicable to real machines during operation. It must be reminded that the possibility of detecting a crack depends highly from the position where the crack has developed, from loads that are applied to the shaft and from the points where the symptoms are measured. Also crack related thermal effects can help in identifying its presence.

Sekhar [8] uses a modal based approach in the time domain, which has been developed by Bach and Markert [9]. Anyhow the method is tested only using numerical results obtained on very simple rotor models, which are unable to represent the behaviour of real machines.

Dilena and Morassi [10] use antiresonances in the frequency response curves of non-rotating beams, while Gounaris and Papadopoulos [11] use the axial vibrations of cracked shafts to detect position and depth of cracks. However, industrial rotating machinery are generally not equipped with sensors able to measure axial vibration. Thus both methods seem unsuitable to detect cracks in rotating machinery during operation in industrial plants.

Other approaches are presented by Dong et. al., who use the deflections of the first mode shape at two symmetric points and the contour diagram of crack location versus crack depth for the first two normalized eigenfrequencies [12]. Also this method can be hardly applied on real machines. Seibold and Weinert [13] use banks of Kalman filters in the time domain on measured vibrations to identify crack depth and localization, but the method requires the definition of large number of banks of filters depending on the accuracy of crack location and depth identification. Another similar application is presented in Bucher and Seibold [14].

The dynamical behaviour of rotors with transverse crack has been studied by many authors (extensive surveys are given in [15]-[17]) and some typical symptoms of crack are well known in a rotating shaft of a machine equipped with standard sensors: a change in 1x rev., 2x rev. and 3x rev vibration vector is suspect. A change in vibration vector means not just an increase or a decrease in amplitude, but also a change in phase only with constant amplitude. However, 1x rev. components can be caused by many other faults (e.g. unbalance, bow, coupling misalignments) and 2x rev. components can be due also to polar stiffness asymmetries (in generators), to surface geometry errors (journal ovalization) and to non-linear effects in oil film bearings. These two last causes can also generate 3x rev. components.

It is then extremely important to have a reference situation, stored by the monitoring system, in which the behaviour of the rotor system without faults and in similar operating conditions is analyzed. The reference situation, better than by a steady state condition at normal operating speed, is represented by run-down transient which furnishes much more information about its dynamical behaviour. By comparing then the actual behaviour during a run-down transient with the reference behaviour, the change in vibrations can be evaluated

and by means of one of the automatic diagnostic procedures based on fault-symptom matrices or on decision trees approach, the type of the most probable impending fault can be identified. Once the type of fault has been identified in a shaft line, also its most probable position and its severity should be identified. This is then possible by means of the least square approach in the frequency domain, which is described in the following.

The method is validated on a test rig specially designed for analyzing the dynamical behaviour of horizontal cracked rotors. Three types of crack are taken into account: the first type is a slot of 34% depth, which is not actually a crack and has not the typical breathing behaviour and which excites significantly only the 2x rev. component. Even if this situation does not generally reproduce a developing crack in a real machine, it is in any case interesting since many papers in literature take into consideration a slot, because the generation of a real fatigue crack in a shaft is a difficult (and expensive) task. The second case, a 14% partially breathing crack is much more interesting in real application since it represents a crack in the early stage of its development; the possibility of early detection of smaller cracks increases the safety of the plant and allows to undertake corrective action. The third case, relative to a about half diameter crack (47%) represents a rotor operating in a dangerous situation, in which the rotor condition is rather close to safety threshold. From this point of view it is very interesting to be able to establish, from vibration measurements during normal operation only, the real depth of the crack.

2 MODEL BASED IDENTIFICATION

Using the approach firstly outlined in [18], the method has been developed and presented in [19]. As described in [20], assuming a finite beam element model for the rotor, the effect of a crack on the statical and dynamical behavior of the rotor can be simulated in the frequency domain, by applying to the rotor different sets of equivalent forces in correspondence of the cracked beam element, one set for each one of the three harmonic components. It can be shown that the overall behaviour of an horizontal axis heavy cracked shaft is linear. Only in extreme operating conditions, the non-linear effect of the breathing crack, which is weak in normal conditions, may influence its behaviour.

The problem of the identification of the position of the crack is then reduced to an external force identification procedure, described in [21].

The stiffness of a cracked shaft is periodical due to the breathing and the rotation of the crack. The Fourier's expansion of the periodical stiffness is truncated in correspondence of the third harmonic component:

$$[\mathbf{K}(\Omega t)] = [\mathbf{K}_m] + [\Delta\mathbf{K}_1]e^{i\Omega t} + [\Delta\mathbf{K}_2]e^{i2\Omega t} + [\Delta\mathbf{K}_3]e^{i3\Omega t} + \dots \quad (1)$$

The elements of $[\Delta\mathbf{K}_n]$ are different from 0 only in the positions corresponding to the cracked element nodes. Introducing this stiffness in the equations of motion of the rotor, eq.(2) is obtained:

$$[\mathbf{M}]\ddot{\mathbf{x}}_t + [\mathbf{C}]\dot{\mathbf{x}}_t + \left([\mathbf{K}_m] + \sum_{j=1}^3 [\Delta\mathbf{K}_j]e^{ij\Omega t} \right) \mathbf{x}_t = \mathbf{F}_e + \mathbf{W} \quad (2)$$

where Ω is the rotating speed, $[\mathbf{M}]$ is the mass matrix, $[\mathbf{C}]$ the damping matrix (including gyroscopic effects), \mathbf{F}_e the external rotating forces (unbalance, bow, etc.) and \mathbf{W} is the statical force vector (weight and so on). The displacement \mathbf{x}_t can be split in its statical \mathbf{x}_s and dynamical \mathbf{x} components:

$$\mathbf{x}_t = \mathbf{x}_s + \mathbf{x} \quad (3)$$

where the static component is given by:

$$\mathbf{x}_s = [\mathbf{K}_m]^{-1} \mathbf{W} \quad (4)$$

According to eq.(3), eq.(5) is finally obtained.

$$[\mathbf{M}]\ddot{\mathbf{x}} + [\mathbf{C}]\dot{\mathbf{x}} + [\mathbf{K}_m]\mathbf{x} = \mathbf{F}_e - \sum_{j=1}^3 [\Delta\mathbf{K}_j] e^{ij\Omega t} (\mathbf{x}_s + \mathbf{x}) \quad (5)$$

If the n -th harmonic component of the vibration \mathbf{x} is taken into account, it can be expressed as:

$$\text{Re}(\mathbf{x}_n e^{in\Omega t}) = \frac{1}{2} \mathbf{x}_n e^{in\Omega t} + \frac{1}{2} \mathbf{x}_n^* e^{-in\Omega t} \quad (6)$$

Similarly, the n -th component of Fourier's expansion of the periodical stiffness $[\Delta\mathbf{K}_n]$ is given by:

$$\text{Re}([\Delta\mathbf{K}_n] e^{in\Omega t}) = \frac{1}{2} [\Delta\mathbf{K}_n] e^{in\Omega t} + \frac{1}{2} [\Delta\mathbf{K}_n^*] e^{-in\Omega t} \quad (7)$$

The Fourier's expansion of both eqs. (6) and (7) is limited to the third harmonic component. If also the product in the last term of eq. (5) is limited to the third harmonic component, then the following equivalent force component vectors are obtained:

$$\widehat{\mathbf{F}}_{f_0} = -\left(\frac{1}{4} [\Delta\mathbf{K}_1] \mathbf{x}_1^* + \frac{1}{4} [\Delta\mathbf{K}_1^*] \mathbf{x}_1 + \frac{1}{4} [\Delta\mathbf{K}_2] \mathbf{x}_2^* + \frac{1}{4} [\Delta\mathbf{K}_2^*] \mathbf{x}_2 + \frac{1}{4} [\Delta\mathbf{K}_3] \mathbf{x}_3^* + \frac{1}{4} [\Delta\mathbf{K}_3^*] \mathbf{x}_3 \right) \quad (8)$$

$$\widehat{\mathbf{F}}_{f_1} e^{i\Omega t} = -\left([\Delta\mathbf{K}_1] \mathbf{x}_s + \frac{1}{2} [\Delta\mathbf{K}_2] \mathbf{x}_1^* + \frac{1}{2} [\Delta\mathbf{K}_3] \mathbf{x}_2^* + \frac{1}{2} [\Delta\mathbf{K}_1^*] \mathbf{x}_2 + \frac{1}{2} [\Delta\mathbf{K}_2^*] \mathbf{x}_3 \right) e^{i\Omega t} \quad (9)$$

$$\widehat{\mathbf{F}}_{f_2} e^{i2\Omega t} = -\left([\Delta\mathbf{K}_2] \mathbf{x}_s + \frac{1}{2} [\Delta\mathbf{K}_3] \mathbf{x}_1^* + \frac{1}{2} [\Delta\mathbf{K}_1] \mathbf{x}_1 + \frac{1}{2} [\Delta\mathbf{K}_1^*] \mathbf{x}_3 \right) e^{i2\Omega t} \quad (10)$$

$$\widehat{\mathbf{F}}_{f_3} e^{i3\Omega t} = -\left([\Delta\mathbf{K}_3] \mathbf{x}_s + \frac{1}{2} [\Delta\mathbf{K}_1] \mathbf{x}_2 + \frac{1}{2} [\Delta\mathbf{K}_2] \mathbf{x}_1 \right) e^{i3\Omega t} \quad (11)$$

of which eqs. (9), (10) and (11) are respectively the first, the second and the third harmonic components of the crack force system. Note that the projections along reference axes of the harmonic component of the force system are not necessarily equal, thus the force system is not in general represented by rotating forces.

From the experimental point of view and under the previously exposed hypothesis of linearity, the difference $\mathbf{x}_a = \mathbf{x}_{total} - \mathbf{x}_{ref.}$, between the measured vibration \mathbf{x}_{total} of a rotor system that has a fault and the reference case $\mathbf{x}_{ref.}$, represents the vibrational behaviour due to the fault, which is called sometimes *additional vibrations*. These vibrations are used in the identification procedure, since they are due to the impending fault only. In fact, the reference case vibrations $\mathbf{x}_{ref.}$ are given by eq. (12):

$$[\mathbf{M}]\ddot{\mathbf{x}}_{ref.} + [\mathbf{C}]\dot{\mathbf{x}}_{ref.} + [\mathbf{K}]\mathbf{x}_{ref.} = \mathbf{F}_e \quad (12)$$

while those caused by the developing crack are given by:

$$[\mathbf{M}]\ddot{\mathbf{x}}_{total} + [\mathbf{C}]\dot{\mathbf{x}}_{total} + [\mathbf{K}_m]\mathbf{x}_{total} = \mathbf{F}_e + \widehat{\mathbf{F}}_{f_0} + \widehat{\mathbf{F}}_{f_1} e^{i\Omega t} + \widehat{\mathbf{F}}_{f_2} e^{i2\Omega t} + \widehat{\mathbf{F}}_{f_3} e^{i3\Omega t} \quad (13)$$

If eq. (13) is considered for an unknown crack, also $[\mathbf{K}_m]$ is unknown. Anyhow it can be approximated by $[\mathbf{K}]$ of the uncracked shaft, from which it differs only very little: the crack affects the stiffness of one element only. Therefore the additional vibrations are given by:

$$[\mathbf{M}]\ddot{\mathbf{x}}_a + [\mathbf{C}]\dot{\mathbf{x}}_a + [\mathbf{K}]\mathbf{x}_a = \widehat{\mathbf{F}}_{f_0} + \widehat{\mathbf{F}}_{f_1} e^{i\Omega t} + \widehat{\mathbf{F}}_{f_2} e^{i2\Omega t} + \widehat{\mathbf{F}}_{f_3} e^{i3\Omega t} \quad (14)$$

By applying the harmonic balance criteria in the frequency domain and considering the additional vibrations \mathbf{X}_n , the following equations are obtained for each harmonic component:

$$\left[-(n\Omega)^2 \mathbf{M} + in\Omega \mathbf{C} + \mathbf{K} \right] \mathbf{X}_n = \mathbf{F}_{f_n} \quad n = 1, 2, 3 \quad (15)$$

in which the force vector \mathbf{F}_{f_n} , has to be identified. For sake of clarity and simplicity, a single fault is considered, while multiple faults can be handled using the method fully described in [21].

In the r.h.s. of eq. (15), the equivalent force system is applied to the two nodes of the element that contains the crack and is therefore composed by a vector of eight generalized forces, in case of 4 degrees of freedoms (d.o.f.s) per node model. Due to energy considerations, it results that the most important among these forces are the bending moments which are roughly equal and opposite on the two nodes of the cracked element. In fact, cracks develop and propagate mainly to axial stresses generated by bending moments in rotating shafts; therefore generally huge bending moments are present in correspondence of cracked elements. Further, it can be shown that in a beam element loaded by shear forces and bending moments, the elastic deflection energy associated to the shear forces is much smaller than the energy associated to the bending moments. Therefore the first one is often neglected in comparison to the second one, as it has been done in the Bernoulli's beam in comparison to the Timoshenko's beam. For this reason, the additional deflections due to the crack can be attributed to equivalent bending moments only.

Therefore the set of equivalent forces in the case of a crack is reduced to a couple of bending moments (with their relative phase) along two orthogonal directions for each n -th harmonic component. The final equations are recalled here below.

The equivalent force system acts on few d.o.f. of the system, therefore vectors $\mathbf{F}_{f_n}^{(x)}$ and $\mathbf{F}_{f_n}^{(y)}$, respectively each one of the reference system directions, are not full-element vectors that are convenient to be represented by means of:

$$\mathbf{F}_{f_n}^{(x,y)} = \left\{ \mathbf{F}_L^{(x,y)} \right\} \overline{A}^{(x,y)} \quad (16)$$

where $\left\{ \mathbf{F}_L^{(x,y)} \right\}$ is the localisation vector which has all null-elements except for the d.o.f. to which the forcing system is applied, and $\overline{A}^{(x,y)}$ is a complex number representing the amplitude and the phase of the fault.

In the case considered in the paper, in which a crack is going to be identified, the three first harmonic components of the vibration are considered. For a crack located in the j -th element of the shaft line, the corresponding equivalent force systems are:

$$\begin{aligned}
\mathbf{F}_{f_n}^{(x)} &= \left\{ \begin{array}{ccccccc} 0 & \vdots & \underbrace{0 \quad i \quad 0 \quad 0}_{j\text{-th rotor node}} & \underbrace{0 \quad -i \quad 0 \quad 0}_{j+1\text{-th rotor node}} & \vdots & 0 & \underbrace{0 \quad \dots \quad 0}_{\text{foundation d.o.f.s}} \end{array} \right\}^T \cdot M_n^{(x)} e^{i\phi_n^{(x)}} = \\
&= \left\{ \mathbf{F}_{L_j}^{(x)} \right\} \bar{A}_n^{(x)}, \quad n=1,2,3 \\
\mathbf{F}_{f_n}^{(y)} &= \left\{ \begin{array}{ccccccc} 0 & \vdots & \underbrace{0 \quad 0 \quad 0 \quad 1}_{j\text{-th rotor node}} & \underbrace{0 \quad 0 \quad 0 \quad -1}_{j+1\text{-th rotor node}} & \vdots & 0 & \underbrace{0 \quad \dots \quad 0}_{\text{foundation d.o.f.s}} \end{array} \right\}^T \cdot M_n^{(y)} e^{i\phi_n^{(y)}} = \\
&= \left\{ \mathbf{F}_{L_j}^{(y)} \right\} \bar{A}_n^{(y)}, \quad n=1,2,3
\end{aligned} \tag{17}$$

where the only terms different from zero are those relative respectively to the rotational horizontal and vertical d.o.f.s of the extreme nodes of element j .

Eq. (15) can be now rewritten considering that condition monitoring systems collect data for many rotating speeds, so the additional vibrations are available for several rotating speeds and a set of n_p rotating speeds is considered:

$$\boldsymbol{\Omega} = \left\{ \Omega_1 \quad \Omega_2 \quad \dots \quad \Omega_{n_p} \right\}^T \tag{18}$$

Then, introducing the admittance matrix $[\mathbf{E}(n\boldsymbol{\Omega})]$ of the system:

$$[\mathbf{E}(\boldsymbol{\Omega})] = \left[-(n\boldsymbol{\Omega})^2 \mathbf{M} + in\boldsymbol{\Omega} \mathbf{C} + \mathbf{K} \right] \quad n=1,2,3 \tag{19}$$

eq. (15) becomes:

$$[\mathbf{E}(n\boldsymbol{\Omega})] \mathbf{X}_n = \begin{bmatrix} \mathbf{E}(n\Omega_1) & 0 & 0 & 0 \\ 0 & \mathbf{E}(n\Omega_2) & 0 & 0 \\ \vdots & \vdots & \vdots & \vdots \\ 0 & 0 & 0 & \mathbf{E}(n\Omega_{n_p}) \end{bmatrix} \begin{Bmatrix} \mathbf{X}_n \\ \mathbf{X}_n \\ \vdots \\ \mathbf{X}_n \end{Bmatrix} = \mathbf{F}_{f_n}, \quad n=1,2,3 \tag{20}$$

Anyhow the equivalent force fault identification problem in eq. (20) is overdetermined since the number of the observation (the measured vibrations at different rotating speeds) are greater than the number of the parameters of the fault that have to be identified. The procedure used to solve the problem is the following, by considering that the vibration measuring points in real machines are corresponding to bearing location.

Let the machine model have n_r nodes and n_b bearings in which the vibrations \mathbf{X}_{Bmn} are measured at n_p rotating speeds in two orthogonal directions, and the supporting structure is represented by means of a foundation with n_f d.o.f.s. The fully assembled model d.o.f.s are $(4n_r + n_f)$ while per each rotating speed are measured only $2n_b$ d.o.f.s. Note that n_e , number of elements, is $n_r - 1$.

Since the fault has to be identified not only in its severity but also in its position, in general the procedure has to be repeated per each node of the rotor, unless the research of the fault is limited in a specified interval of the nodes.

Eq. (20) represents the general system of equations for all the d.o.f.s of the considered fully assembled machine. The admittance matrix $[\mathbf{E}(n\boldsymbol{\Omega})]$ has order $((4n_r + n_f)n_p \times (4n_r + n_f)n_p)$.

Now, least square identification is used here in order to evaluate the module, the phase and a residual of the fault, starting from the first element and moving along the rotor from element to element. Weighted least square technique can be employed in order to increase the robustness of the identification as described in [22].

The equivalent force system, is applied in each element of the rotor model, so for all the rotating speeds the fault vector is of order $((4n_r + n_f)n_p \times 2)$. Therefore, in the first element, the localization matrix for the i -th rotating speed is:

$$[\mathbf{F}_{L_i}]^{(i)} = \begin{bmatrix} 0 & i & 0 & 0 & 0 & -i & 0 & 0 & \vdots & 0 & 0 & \cdots & 0 \\ 0 & 0 & 0 & 1 & 0 & 0 & 0 & -1 & \vdots & 0 & 0 & \cdots & 0 \\ \underbrace{\hspace{10em}}_{1^{\text{st}} \text{ rotor node}} & \underbrace{\hspace{10em}}_{2^{\text{nd}} \text{ rotor node}} & \underbrace{\hspace{10em}}_{\text{foundation d.o.f.s}} \end{bmatrix}^T \quad (21)$$

and for all the n_p rotating speeds:

$$\mathbf{F}_{L_i} = \begin{Bmatrix} [\mathbf{F}_{L_i}]^{(1)} \\ \vdots \\ [\mathbf{F}_{L_i}]^{(n_p)} \end{Bmatrix} \quad (22)$$

The effect on the measured d.o.f.s $[\hat{\mathbf{X}}_{B_n}]$, which vector is of order $(2n_b n_p \times 1)$, due to unitary force systems applied to the selected element of the model is now calculated. This is done by first substituting eq. (21) in the right hand side of eq. (20), and inverting matrix $[\mathbf{E}(n\Omega)]$, obtaining the matrix $[\mathbf{H}(n\Omega)]$.

$$\mathbf{X}_n = [\mathbf{E}(n\Omega)]^{-1} \mathbf{F}_{f_n}(\Omega) = [\mathbf{H}(n\Omega)] \mathbf{F}_{L_i}(\Omega), \quad n = 1, 2, 3 \quad (23)$$

Then, the vibrations of the d.o.f.s, which are measured, are separated from the remaining d.o.f.s of the system, by considering only the rows of $[\mathbf{H}(n\Omega)]$ corresponding to the measured d.o.f.s. The partitioned matrix is of order $(2n_b n_p \times (4n_r + n_f)n_p)$ and following eq. (24) is obtained:

$$[\hat{\mathbf{X}}_{B_n}] = [\mathbf{H}(n\Omega)] \Big|_{\substack{\text{measured} \\ \text{d.o.f.s}}} \mathbf{F}_{L_i}, \quad n = 1, 2, 3 \quad (24)$$

Now the complex vector $\bar{\mathbf{A}}_n = \{\bar{A}_n^{(x)} \quad \bar{A}_n^{(y)}\}^T$ (i.e. the module and the phase for each harmonic component) of the equivalent force systems, applied to the selected element, that fits best the experimental data $\mathbf{X}_{B_{m_n}}$, of order $(2n_b n_p \times 1)$, has to be estimated. The fitting is done in least square sense, since the number of the unknown (the module and the phase) is less than the equations (recalling that data are corresponding to several rotating speeds and each of the sets is composed by several measuring planes). The problem is equivalent to:

$$\min \left\| [\hat{\mathbf{X}}_{B_n}] \bar{\mathbf{A}}_n - \mathbf{X}_{B_{m_n}} \right\|, \quad n = 1, 2, 3 \quad (25)$$

whose general solution is given by means of the pseudo-inverse calculation:

$$\bar{\mathbf{A}}_n^{(1)} = \begin{Bmatrix} M_n^{(x),(1)} e^{i\phi_n^{(x),(1)}} \\ M_n^{(y),(1)} e^{i\phi_n^{(y),(1)}} \end{Bmatrix} = \left(\begin{bmatrix} \hat{\mathbf{X}}_{Bn} \end{bmatrix}^T \begin{bmatrix} \hat{\mathbf{X}}_{Bn} \end{bmatrix} \right)^{-1} \begin{bmatrix} \hat{\mathbf{X}}_{Bn} \end{bmatrix}^T \mathbf{X}_{Bm_n}, \quad n=1,2,3 \quad (26)$$

The module and the phase of the complex value in the rows of $\bar{\mathbf{A}}_n^{(1)}$ are the equivalent bending moments due to the crack, in the selected element. Finally the residual in the selected element is determined, by first obtaining the calculated response due to the identified fault in the selected element:

$$\mathbf{X}_{Bn} = \begin{bmatrix} \hat{\mathbf{X}}_{Bn} \end{bmatrix} \bar{\mathbf{A}}_n^{(1)}, \quad n=1,2,3 \quad (27)$$

and then by normalizing it:

$$\delta_{r_n}^{(1)} = \left(\frac{\begin{bmatrix} \mathbf{X}_{Bn} - \mathbf{X}_{Bm_n} \end{bmatrix}^{*T} \begin{bmatrix} \mathbf{X}_{Bn} - \mathbf{X}_{Bm_n} \end{bmatrix}}{\mathbf{X}_{Bm_n}^{*T} \mathbf{X}_{Bm_n}} \right)^{1/2}, \quad n=1,2,3 \quad (28)$$

The procedure is then iterated for all the n_e elements of the rotor. If a fault only is considered, a set in \mathbb{R} of relative residuals given by eq. (28), ordered by the element number, is obtained:

$$\boldsymbol{\delta}_{r_n} = (\delta_{r_n}^{(1)}, \dots, \delta_{r_n}^{(n_r-1)}), \quad n=1,2,3 \quad (29)$$

A graph representing the values of $\boldsymbol{\delta}_{r_n}$ along the shaft axis (from the first to the last element) can be drawn. The location that corresponds to the minimum value of $\boldsymbol{\delta}_{r_n}$ indicates the most probable location of the fault (see figure 21, figure 29 and figure 37), whose estimation is given by the corresponding values $\mathbf{M}_n = M_n^{(x)} e^{i\phi_n^{(x)}} + M_n^{(y)} e^{i\phi_n^{(y)}}$ of eq. (26). The closer to zero the minimum value of eq. (29) is, the better the estimation of the faults is per each harmonic component.

It is worth noting that the 1x rev. vibration components are due both to the breathing mechanism of the crack and to the local bow which generally has developed during the crack propagation. Therefore, when no other sources of bow are present, the 1x rev. component is useful for the localization of the crack, but not for the identification of its depth.

The 3x rev. component is rather small and generally masked by some noise. Often this component can be recognized only when approaching the resonant condition at a rotating speed equal to 1/3 the rotor's critical speed.

The 2x rev. component is therefore the most suitable symptom for detecting position and depth of the crack; the highest values are obviously reached during a run-down transient when approaching the resonant condition at 1/2 critical speed.

The final remark about the model based method regards the accuracy of the machine model. A full discussion would be far from the scope of this paper, but a reader potentially interested in measures of accuracy in model based identification can refer to [23].

3 CRACK DEPTH IDENTIFICATION

The following procedure has been implemented for the identification of the crack depth. The identification procedure, described in the previous section, identifies the crack position in a particular element of the rotor, whose length is known from the f.e.m. and equal to l (figure

1). Figure 1 shows also the crack depth p , the d.o.f.s of the extremity nodes of the element and the bending caused by the *equivalent* moment components \mathbf{M}_n (1x, 2x and 3x rev. components) that are applied to this element. These equivalent bending moment components \mathbf{M}_1 , \mathbf{M}_2 and \mathbf{M}_3 have been calculated from the corresponding 1x, 2x and 3x rev. measured vibrational behavior.

Then the static bending moment \mathbf{M} in correspondence of the same element, due to the weight and to bearing alignment conditions, is calculated from model data.

The moments \mathbf{M}_1 , \mathbf{M}_2 and \mathbf{M}_3 represent the amplitude of the equivalent crack forces defined respectively by eqs. (9), (10) and (11). If we neglect all terms of eqs. (9), (10) and (11) except the first one, we obtain:

$$\mathbf{F}_{f_n} = -[\Delta\mathbf{K}_n]\mathbf{x}_s \quad (30)$$

This assumption is reasonable if heavy, horizontal axis, industrial rotating machinery are considered, since the static deflection, in the shaft sections loaded by consistent bending moments, is much higher than the vibrations, especially when operating conditions far from resonances in critical speeds are analyzed. Moreover, it is possible to show that the projections along the reference axes are equal in case of 2x rev. component, i.e. $M_2^{(x)} = M_2^{(y)} = M_2$ and $\varphi_2^{(x)} = \varphi_2^{(y)}$, and the equivalent force system is a rotating moment of amplitude M_2 .

Even if vector \mathbf{F}_{f_n} has order $(4n_r + n_f) \times 1$, the only elements different from zero are those corresponding to the d.o.f.s of the cracked element j -th. Therefore, it is more convenient to consider only the sub-matrix $[\Delta\mathbf{K}_n]_j$ of order 8×8 corresponding to those d.o.f.s and the displacement vector $\mathbf{x}_s|_j$ of the nodes of the cracked element (figure 1):

$$\mathbf{x}_s|_j = \left\{ \underbrace{x_j \quad \vartheta_{x_j} \quad y_j \quad \vartheta_{y_j}}_{j^{\text{th}} \text{ rotor node}} \quad \underbrace{x_{j+1} \quad \vartheta_{x_{j+1}} \quad y_{j+1} \quad \vartheta_{y_{j+1}}}_{j+1^{\text{th}} \text{ rotor node}} \right\}^T \quad (31)$$

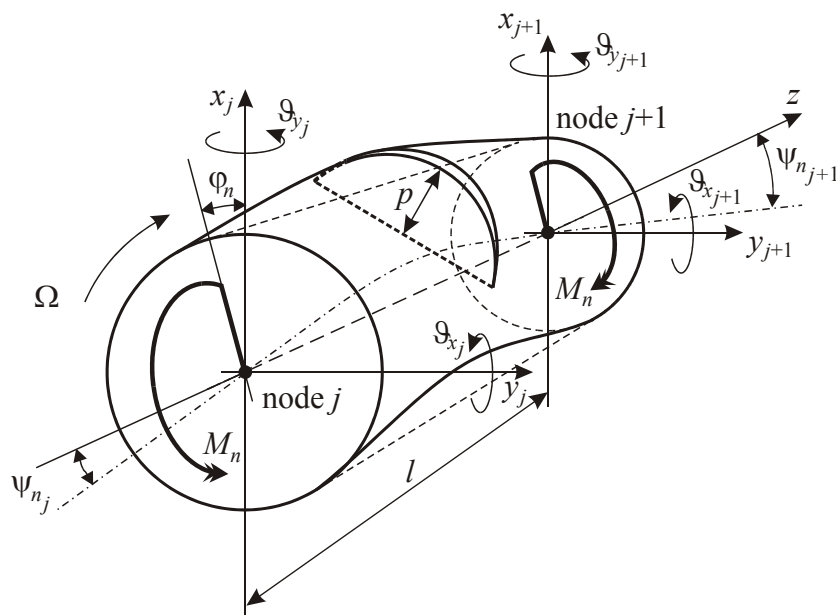


Figure 1. Cracked element.

By recalling eqs. (17) and (30), it follows:

$$\begin{bmatrix} \underbrace{0 & i & 0 & 0}_{j\text{-th rotor node}} & \underbrace{0 & -i & 0 & 0}_{j+1\text{-th rotor node}} \\ \underbrace{0 & 0 & 0 & 1}_{j\text{-th rotor node}} & \underbrace{0 & 0 & 0 & -1}_{j+1\text{-th rotor node}} \end{bmatrix}^T \begin{Bmatrix} M_n^{(x)} e^{i\varphi_n^{(x)}} \\ M_n^{(y)} e^{i\varphi_n^{(y)}} \end{Bmatrix} = -[\Delta\mathbf{K}_n]_j \mathbf{x}_s|_j \quad (32)$$

and for the modulus:

$$M_n = \|\mathbf{M}_2\| = \left\| [\Delta\mathbf{K}_n]_j \mathbf{x}_s|_j \right\| \quad (33)$$

Matrix $[\Delta\mathbf{K}_n]$ is restricted to the nodes of the cracked element, therefore only the statical deflections of the nodes of the cracked element are required in eq. (33). Since in the crack, as in the Bernoulli's beam, the shear force can be neglected with respect to bending moment flexibility, $\mathbf{x}_s|_j$ is composed mainly by rotational deflections of the extremity nodes.

Therefore $\mathbf{x}_s|_j$ can be calculated by considering the statical bending moments due to static, fixed in space, force vector \mathbf{W} acting on the cracked element. These bending moments do not change much from node to node of a element and can therefore be considered constant in the cracked element and equal to M . Moment M is then proportional to the relative rotations of the extremity nodes of the cracked element, $\psi_{j+1} - \psi_j$ (see figure 1).

By considering the sub-matrix $[\mathbf{K}_m]_j$ of order 8×8 corresponding to those d.o.f.s extracted from the matrix $[\mathbf{K}_m]$, i.e. the mean value of the stiffness matrix of the cracked element, the statical deflections of the cracked element are given also by:

$$\mathbf{x}_s|_j = \left([\mathbf{K}_m]_j \right)^{-1} \left\{ \underbrace{0 \quad \cos \varphi_s \quad 0 \quad \sin \varphi_s}_{j\text{-th rotor node}} \quad \underbrace{0 \quad -\cos \varphi_s \quad 0 \quad -\sin \varphi_s}_{j+1\text{-th rotor node}} \right\}^T M \quad (34)$$

By replacing eq. (34) in eq. (33), it finally results:

$$M_n = \left\| [\Delta\mathbf{K}_n]_j \left([\mathbf{K}_m]_j \right)^{-1} \right\| M \rightarrow \frac{M_n}{M} = \left\| [\Delta\mathbf{K}_n]_j \left([\mathbf{K}_m]_j \right)^{-1} \right\| \quad (35)$$

Eq. (35) shows that ratio M_n/M depends only on the crack depth p , since $[\Delta\mathbf{K}_n]_j$ and $[\mathbf{K}_m]_j$ of the cracked element are function of p only, if regular shapes with rectilinear tips are considered.

A similar ratio M'_n/M has been calculated for different cracks depths considering the *equivalent* length l_c of the cracked element, instead of the length l of the cracked element in the model of the shaft. This equivalent length l_c has been tuned by means of numerical 3D analyses (figure 2) as shown in [20] and [24].

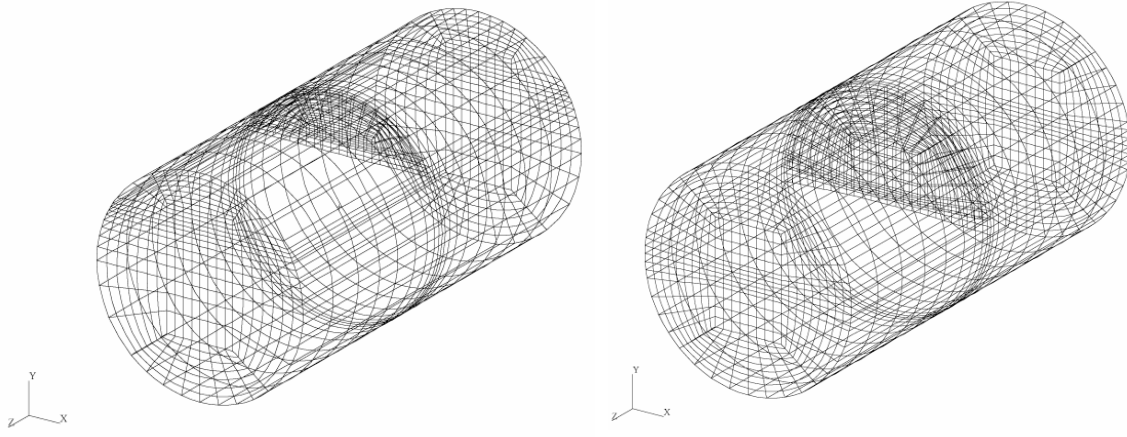


Figure 2. Equivalent cracked beams models used in 3D analyses.

Moment M'_n gives the same relative rotation of the nodes of the beam with length l_c as M_n does with a beam with length l :

$$\Delta\psi_n = \frac{M'_n}{EJ} l_c \quad (36)$$

This is represented in figure 3 for the 1x, 2x and 3x rev. component and expressed by the relationship in eq. (37).

$$\frac{M'_n}{M} = f(p) \quad (37)$$

In the same figure also the curve M'_{2slot}/M for an always open crack (a slot or notch) is shown: in this case the 2x rev. component only is present and 1x and 3x rev. component are absent.

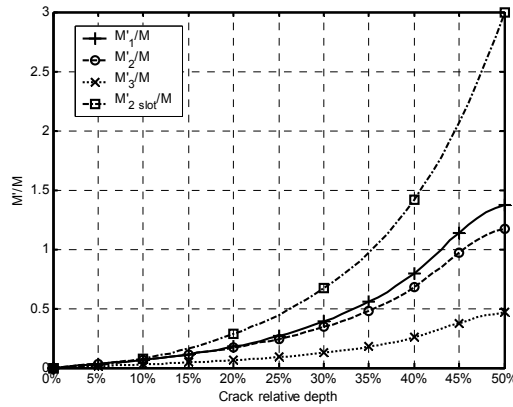


Figure 3. Bending moments ratio on the equivalent cracked beam, as a function of crack relative depth for the nx rev. component.

Eq. (37) can then be used for determining the crack depth. However, as shown in [20], the length l_c of the *equivalent*, reduced stiffness, beam element that simulates the behavior of the cracked beam, is also depending on the relative crack depth p :

$$\frac{l_c}{D} = g(p) \quad (38)$$

The function $g(p)$ is represented in figure 4. Anyhow, coming from the identification procedure, the equivalent bending moments M_n are applied to an element with an actual length l instead of l_c . It is worth noting that the nx rev. measured displacements are the effect of the relative rotation of the cracked element extremity nodes, which is proportional to the product $M_n \cdot l$ of the identified nx rev. bending moment component M_n applied to one element of the finite element (f.e.) model of the rotor, multiplied by its length l .

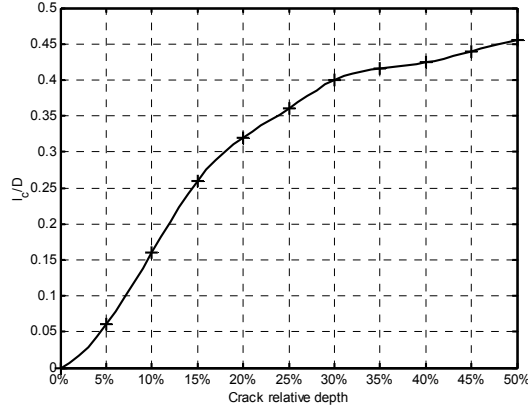


Figure 4. Relationship between the crack relative depth p , the diameter D and the length l_c of equivalent beam.

The equivalent bending moment component M'_n , applied to an equivalent cracked beam element of length l_c , can therefore be calculated as:

$$M'_n \cdot l_c = M_n \cdot l \quad (39)$$

By assuming that the statical bending moment M applied to the original element of length l does not change along the element, the same M can be considered applied to the element with equivalent length l_c . Recalling eq. (37) we can derive:

$$\frac{M'_n}{M} = \frac{M_n \cdot l}{M \cdot l_c} = f(p) \quad (40)$$

and using eq. (38) we get:

$$\frac{M_n \cdot l}{M \cdot D} = f(p) \cdot g(p) \quad (41)$$

Eq. (41), shown in figure 5 for the nx rev. components, can then be used for determining, from the known left hand side, the relative depth of the crack.

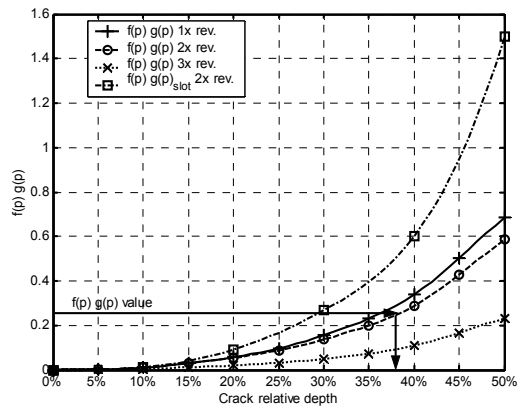


Figure 5. Function for the calculation of the crack depth.

4 EXPERIMENTAL RESULTS

4.1 Test rig assembly

The test rig EUROPE of EDF (Electricité de France), shown in figure 6, is composed by a shaft divided in three parts supported by two equal oil film bearings. The bearings are three lobed shape. The nominal diameter of the shaft is 70 mm and the overall length is 3.15 m. The distance between the bearings is 1.88 m. The total mass is 450 kg and the main inertia disk has a mass of 250 kg. In this configuration the 1st critical speed is close to 1150 rpm. The supporting structure can be considered as rigid in the speed range 0-1500 rpm. The proximity probes for the measurements of relative shaft-journal vibrations are installed very close to the bearings, but not inside of them, as usually occurs in real machines (in figure 6, they are both on the bearing side towards the motor). The test rig has been designed in order to be as much as possible representative of industrial machines, mainly steam turbines of power plants.

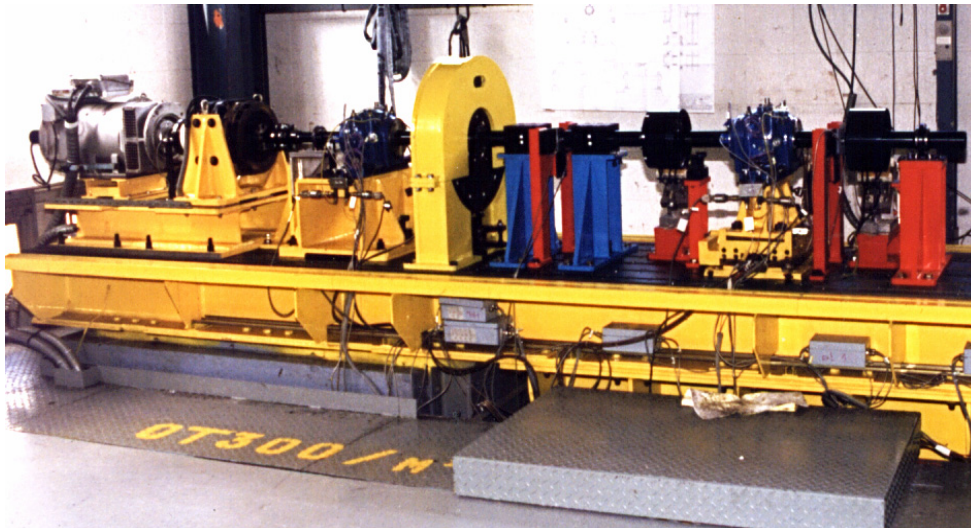


Figure 6. 2-bearing 1-composed shaft test rig on rigid foundation

Maximum design speed is 3000 rpm. In this application for safety reasons, the maximum speed was reduced to 1500 rpm. The last is also the operating speed of turbo-groups of many nuclear power plants, equipped with 4 poles generators.

The model of the rotor is shown in figure 7 and is composed 45 finite beam elements.

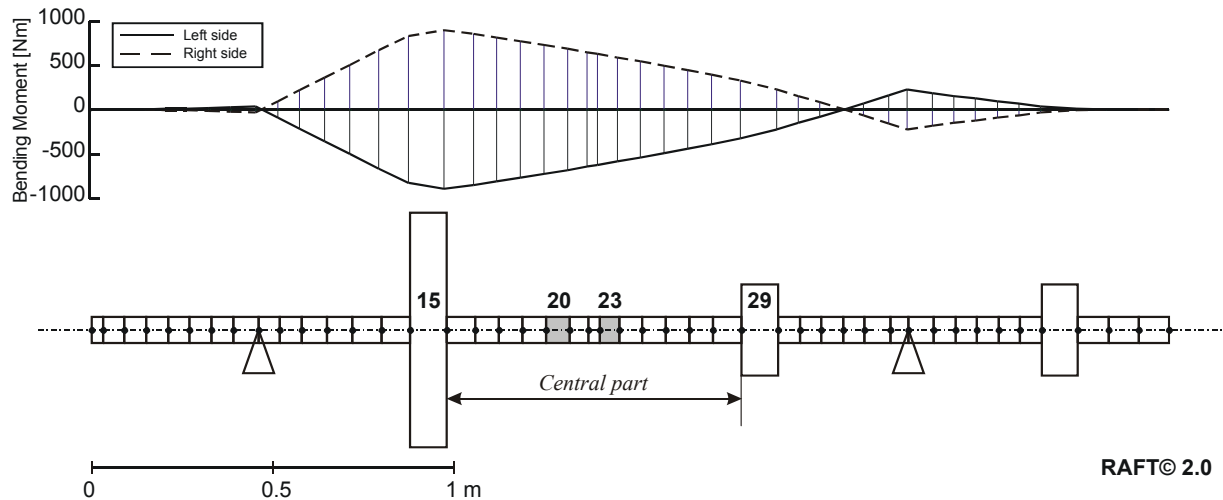


Figure 7. Finite beam element model of the test rig and static bending moment distribution.

Since the central part of the rotor, between elements 15 and 29, can be disassembled, three types of crack were generated on three different specimens, assembled in the rotor system, and used for validating the identification procedure.

In the first case a transverse slot of thickness 0.1 mm and of relative depth of 34% was generated by electroerosion, at a distance of 310 mm from the main inertia disk. This position corresponds roughly to element 20 in the finite beam element model of the rotor (figure 7).

In the second case, starting from a notch made by electroerosion, a crack was obtained as a consequence of fatigue solicitation. The crack position along the rotor corresponds again to element 20. At the end of the tests this last shaft was broken to check the actual shape and depth of the crack. From the analysis of figure 8, the crack average depth results of only about 14% with a maximum depth of 11.3 mm equal to 16.1%, but a relevant part of this depth is due to the notch.

In the third case, the crack has been started from a notch and made grown up to an average depth of 33 mm, checked at the end of the tests. This depth corresponds to 47% of the shaft of 70 mm of diameter. The distance was of 430 mm from the main inertia disk, that corresponds to element 23 (figure 7).

The possibility of disassembling of the central part of the rotor has the main advantage to not dismount the entire rotor in order to create a crack. However this leads to some difficulties to have a valid reference case. In fact, by considering a run-down of the uncracked rotor and a run-down of a cracked one, small differences in alignment might be introduced when the central part is coupled to the other extremities. Moreover, the cracked part presents usually a permanent bow due to the fatigue solicitation used to generate the crack. This bow is generally different from that present in the reference case.

The static bending moments are shown in figure 7. Note that the solid line represents the moments on the left side of the element, while the dashed line the moments on the right side.

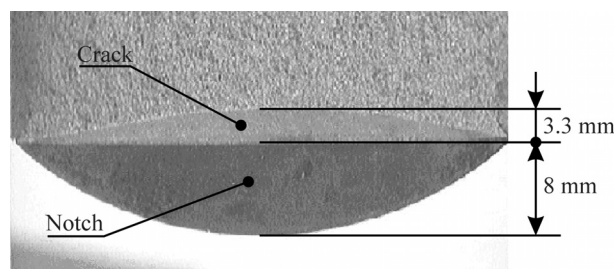


Figure 8. Mean crack depth of 14% in the second experimental case.

4.2 Reference situation

Even if the so-called *reference situation* cannot actually be considered as the true reference situation of the same rotor in this test rig, due to the reason previously expressed, nevertheless it has been used to calculate the vibration difference. The measured reference situation is reported in figure 9 to figure 14 for the 1x, 2x and 3x rev. components.

From the analysis of the 1x rev. component in figure 9 and figure 10, the 1st critical speed at about 1150 rpm is recognizable. Moreover, the rotor presents a bow which generates around 15 μm at very low speed in bearing 1.

In regards to the 2x rev. component in figure 11 and figure 12, the 2x rev. critical speed is rather evident at about 1/2 of the 1st critical speed, but also a peak at about 1100 rpm that indicates a non linear effect of the oil film can be recognized. The relatively high value of the 2x rev. component in the second bearing (about 14 μm) at low speed, which remains the main component over all the speed range as is also shown by the phase trend, indicates a geometrical error of the shaft (journal ovalization) in the bearing. The phase difference of 180° between horizontal and vertical components is typical for ovalization errors. The 3x rev. component has very reduced amplitude in both bearings (about 1 μm and 4 μm respectively) and is mainly due to some noise, however a smaller peak at about 1/3 of the 1st critical speed is recognizable.

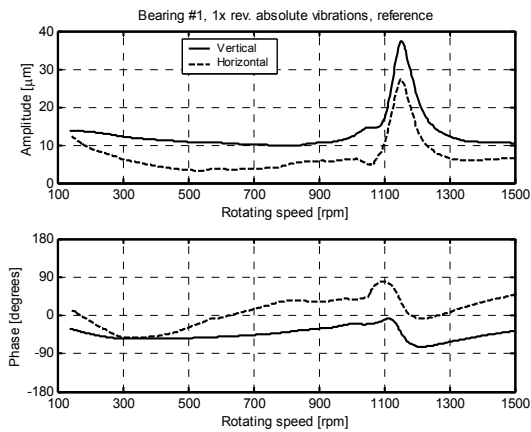


Figure 9. Reference case: 1x rev. vibration components for bearing 1.

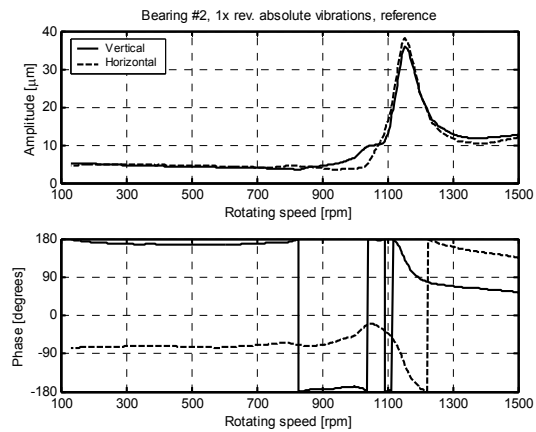


Figure 10. Reference case: 1x rev. vibration components for bearing 2.

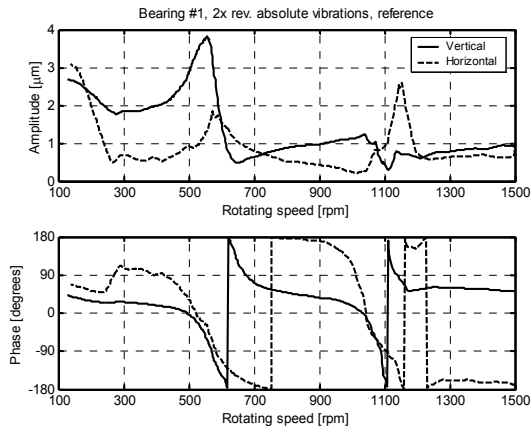


Figure 11. Reference case: 2x rev. vibration components for bearing 1.

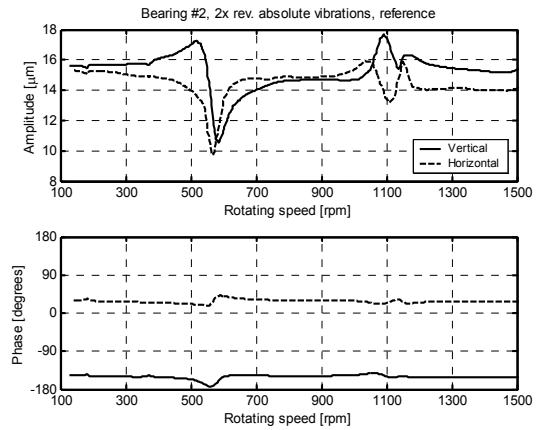


Figure 12. Reference case: 2x rev. vibration components for bearing 2.

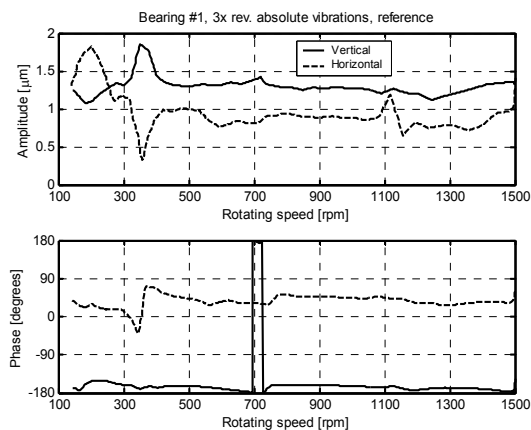


Figure 13. Reference case: 3x rev. vibration components for bearing 1.

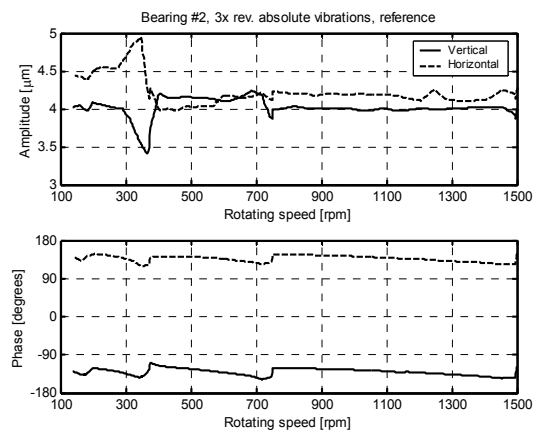
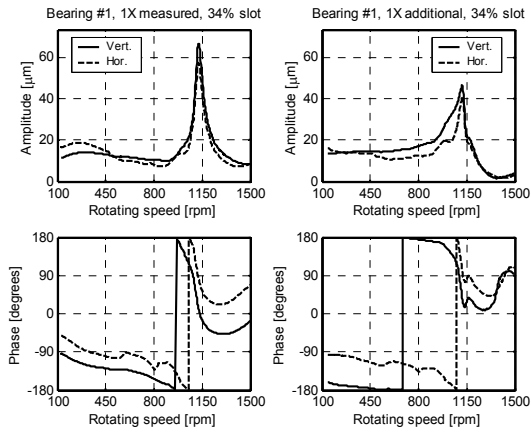


Figure 14. Reference case: 3x rev. vibration components for bearing 2.

4.3 Case 1: identification of a 34% slot.

The measured and the additional vibrations in the bearings, i.e. the differences between the measured vibrations in the sensor positions in the reference case and in the case of the slot, for the first three harmonic components in the case of a 34% slot are reported in figure 15 to figure 20. Since the slot is practically an always open crack, it does not present a breathing behavior and the only significant contribution, which is not due to the unassembly/reassembly of the rotor, is due to the rotor stiffness unsymmetry which occurs twice per revolution. Therefore, only the 2x rev. additional vibrations will be considered in the identification procedure.

In regards to the 1x rev. components, a significant offset is present in both the bearing at very low rotating speeds, that indicates again a permanent bow in the rotor. The 3x rev. components are rather small and the peak at 1/3 of the 1st critical speed is not present in all the measured vibrations.



**Figure 15. Case 1, 34% slot (open crack):
1x rev. vibration components for bearing
1.**

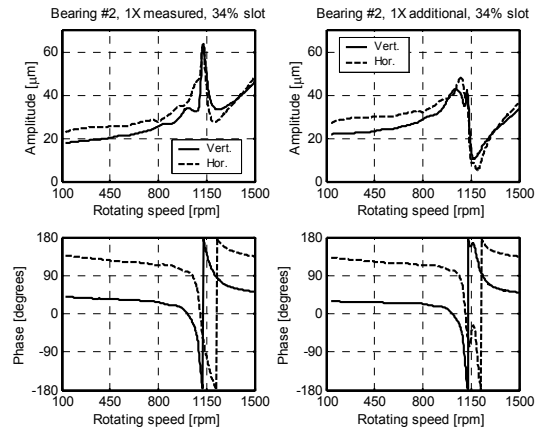


**Figure 16. Case 1, 34% slot (open crack):
1x rev. vibration components for bearing
2.**

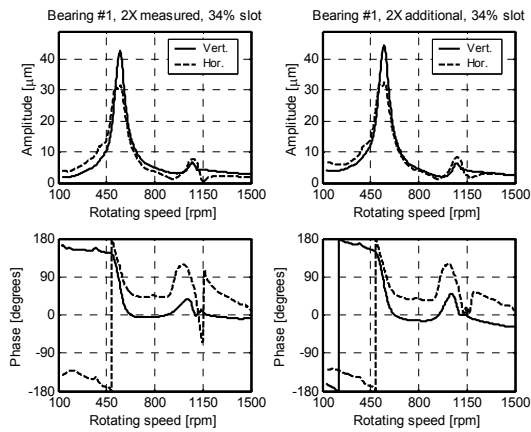


**Figure 17. Case 1, 34% slot (open crack):
2x rev. vibration components for bearing
1.**

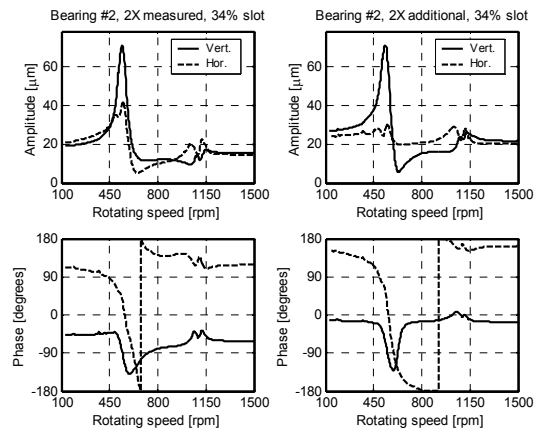


**Figure 18. Case 1, 34% slot (open crack):
2x rev. vibration components for bearing
2.**

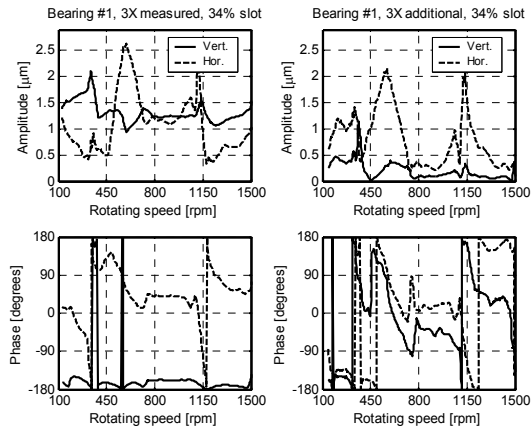


Figure 19. Case 1, 34% slot (open crack): 3x rev. vibration components for bearing 1.

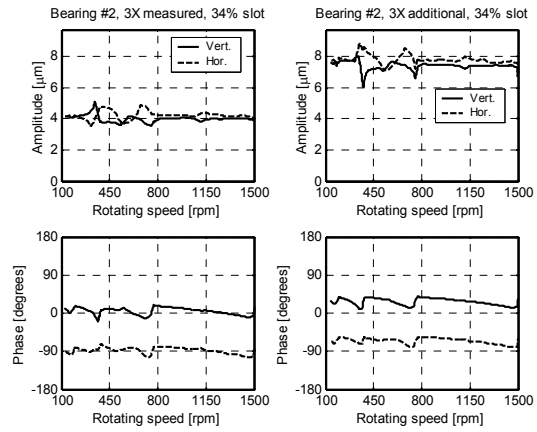


Figure 20. Case 1, 34% slot (open crack): 3x rev. vibration components for bearing 2.

The identification results (using the additional vibration at all the available rotating speeds) are shown in figure 21, taking into account that in this case the M'_{2slot} / M curve of figure 5 is used. The M_{2slot} identified moment is equal to 218 Nm, while the statical bending moment M is 727 Nm (see figure 7) in element 19. Taking into account that shaft diameter D is 70 mm and element 19 length l is 65 mm, the right hand side (r.h.s.) of eq. (41) is 0.278, that corresponds in figure 5 to a depth of about 32%.

The relative residual curve has its minimum in a position in the f.e. model of the rotor, which is very close to the actual crack position, with an error equal to 2.1% with respect to the overall length of the rotor. The depth is almost correctly estimated. A further confirmation is reported in figure 22, in which the comparison between the 2x rev. measured additional vibration in bearing 1 are compared with the calculated ones using the identified equivalent bending moments. Similar results are obtained for the other direction and the other bearing.

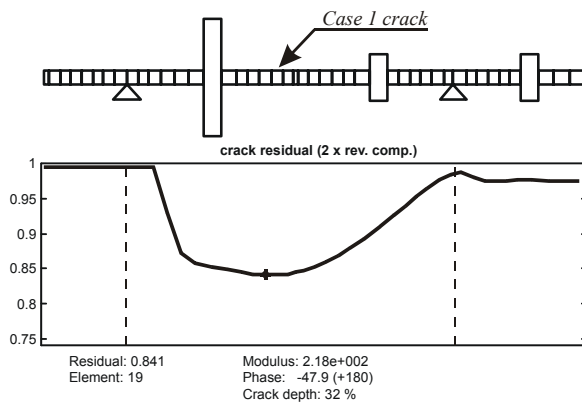


Figure 21. Case 1, 34% slot (open crack): relative residual of the fault identified from 2x rev. component.

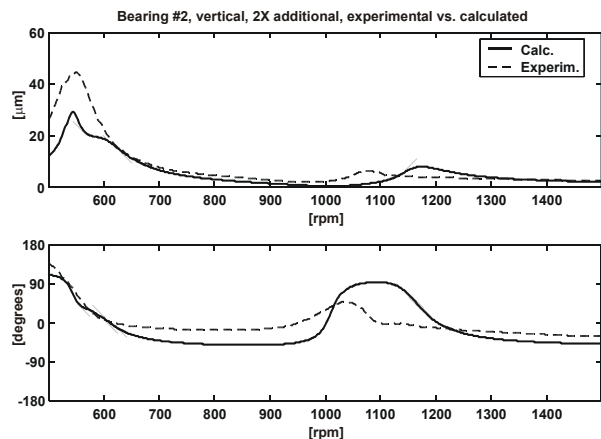


Figure 22. Case 1, 34% slot (open crack): comparison of additional and calculated 2x rev displacements in bearing 1.

4.4 Case 2: identification of a 14% crack.

The additional vibrations in the bearings for the first three harmonic components in this case are reported in figure 23 to figure 28.

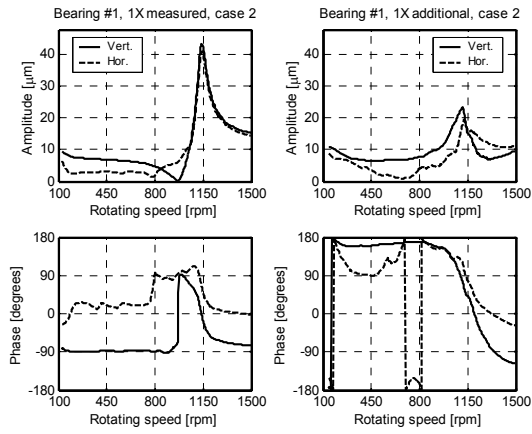


Figure 23. Case 2, slot & crack: 1x rev. vibration components for bearing 1.

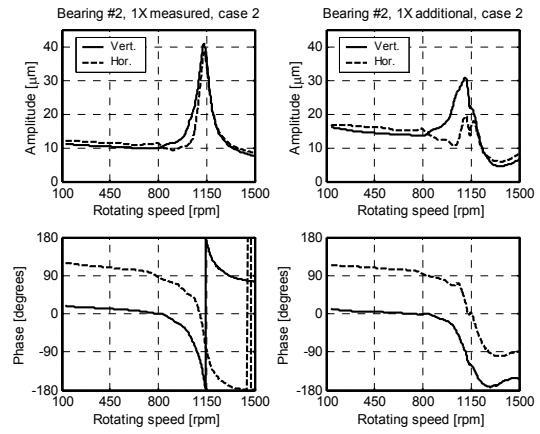


Figure 24. Case 2, slot & crack: 1x rev. vibration components for bearing 2.

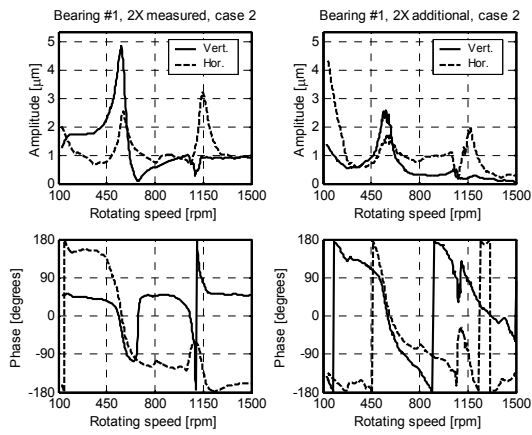


Figure 25. Case 2, slot & crack: 2x rev. vibration components for bearing 1.

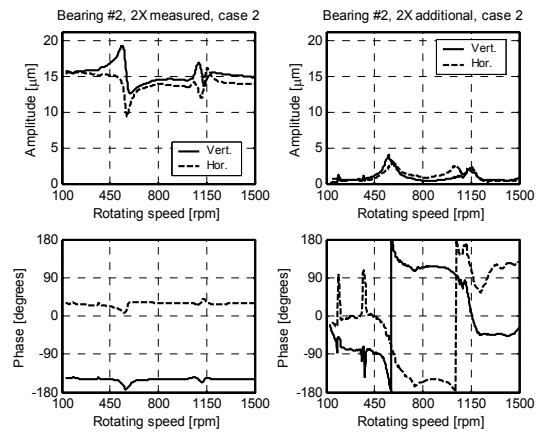


Figure 26. Case 2, slot & crack: 2x rev. vibration components for bearing 2.

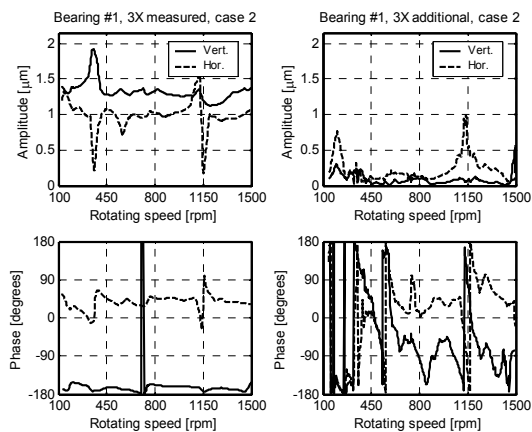


Figure 27. Case 2, slot & crack: 3x rev. vibration components for bearing 1.

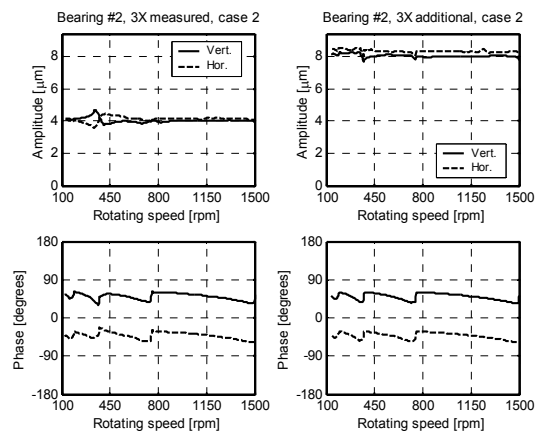


Figure 28. Case 2, slot & crack: 3x rev. vibration components for bearing 2.

The 1x rev. behavior shows a high run-out at low speed, due to a permanent bow of the rotor. The 3x rev. component, instead, is rather high and constant in amplitude and phase which

could indicate geometrical surface errors. As already stressed, in this case the crack is not properly a real crack, nor a slot, since it is breathing only for a smaller part of its surface (see figure 8), but the two curves M'_{2slot}/M and M'_2/M of figure 5 are very close to each other when the depth is small, so the curve relative to an actual crack is used. The results of the identification for the 2x rev. component are reported in figure 29. The M_2 is equal to 19 Nm, while the statical bending moment M is equal to 684 Nm in element 20 (figure 7). Since the shaft diameter D is 70 mm and element 20 length l is 65 mm, the r.h.s. of eq. (41) is 0.026, that corresponds in figure 5 to a depth of 15.6%.

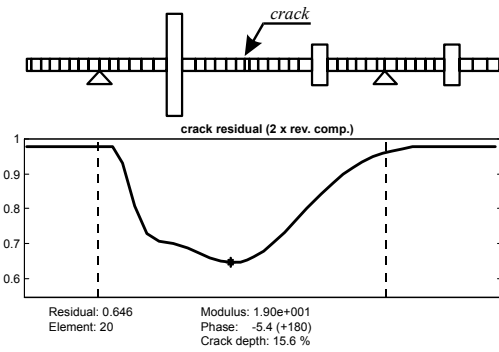


Figure 29. Case 2, slot & crack: relative residual of the fault identified from 2x rev. component.

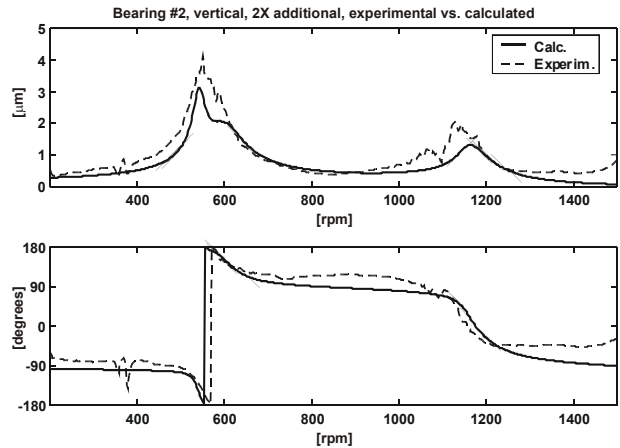


Figure 30. Case 2, slot & crack: 2x rev. measured and calculated vertical displacements close to bearing 2.

The position of the crack, and also its relative depth is identified with good accuracy by means of the 2x rev. component (Figure 29). The identification is not shown for 1x and 3x rev. components, due to the unknown bow for the 1x rev. and to the noise for the 3x rev. components.

Finally the comparison between the experimental and the calculated values (with the identified couples) in the measuring positions are shown in Figure 30 for the 2x rev. component, in vertical direction, close to bearing 2.

Despite the fact that the small crack (about 14%) generates only small 2x rev. additional vibration components, less than $2 \mu\text{m}$ in bearing 1 and less than $5 \mu\text{m}$ in bearing 2, the identification can be considered successful. Figure 30 shows that the fitting of the calculated results to the experimental ones is rather good.

4.5 Case 3: identification of a 47% crack.

The additional vibrations obtained with a crack of about 47% depth of the diameter in the central section are shown in figure 31-figure 36.

From the 1x rev. component (figure 31 and figure 32) it can be inferred that the rotor presents a permanent bow which is increased with respect to the reference rotor. In regards to the 2x rev. component, the high amplitude (about $40\text{-}50 \mu\text{m}$) of the peak at $1/2$ of the 1st critical speed is clearly due to the crack, which produces also a high resonance amplitude (about $10 \mu\text{m}$) of the 3x rev. component at $1/3$ of the 1st critical speed.

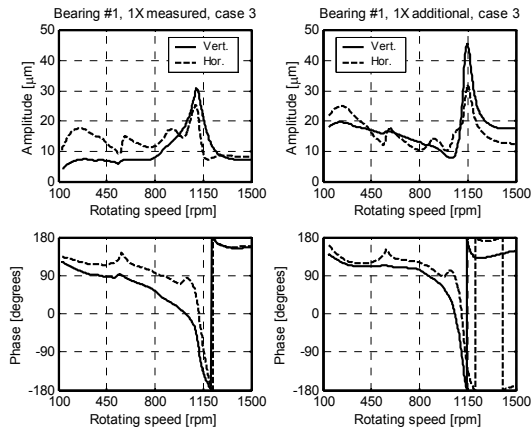


Figure 31. Case 3, crack: 1x rev. vibration components for bearing 1.

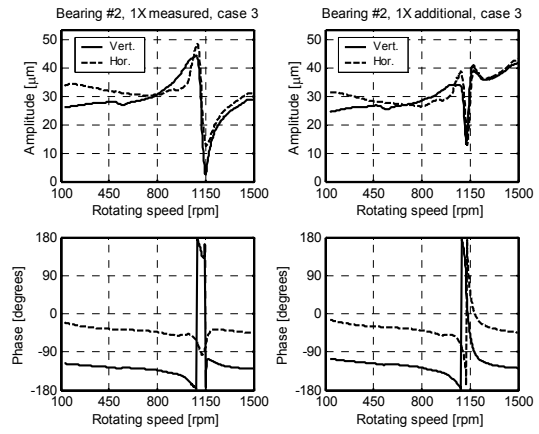


Figure 32. Case 3, crack: 1x rev. vibration components for bearing 2.

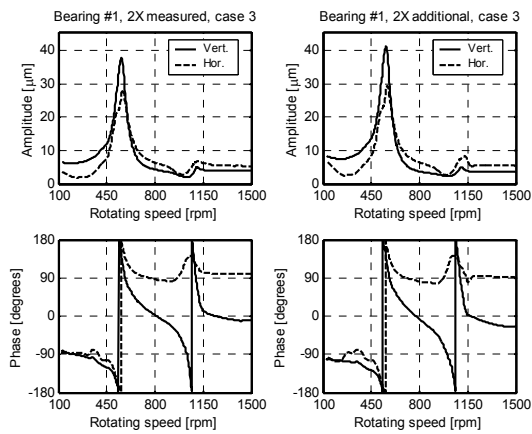


Figure 33. Case 3, crack: 2x rev. vibration components for bearing 1.

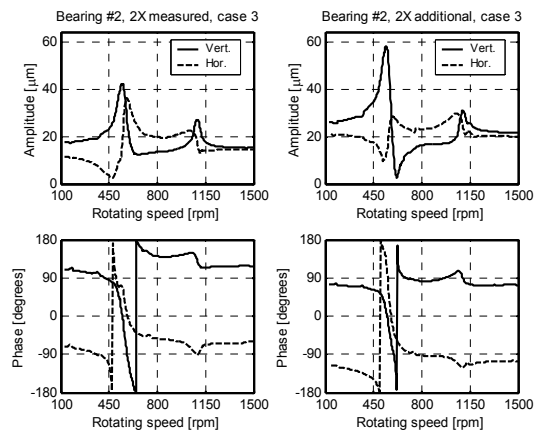


Figure 34. Case 3, crack: 2x rev. vibration components for bearing 2.

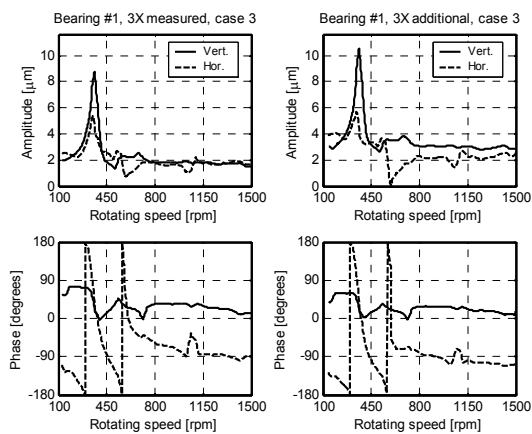


Figure 35. Case 3, crack: 3x rev. vibration components for bearing 1.

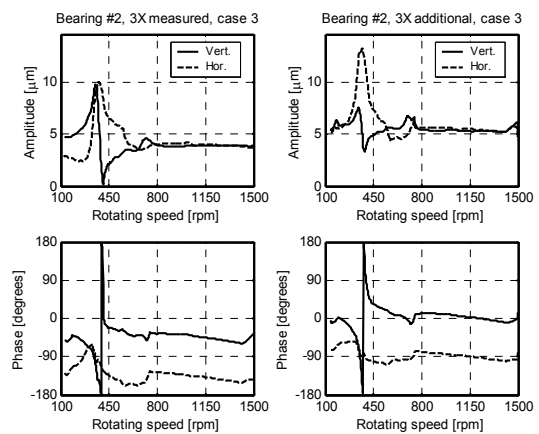


Figure 36. Case 3, crack: 3x rev. vibration components for bearing 2.

In this case the identification of the crack has been attempted not only by using the 2x rev. component, but also by the 1x rev. and 3x rev. components. In fact the last one has a rather

high value, while some processing were used in order to depurate the effect of the unbalance in the 1x rev. component as explained later.

The results in figure 37 show that the location of the crack is precisely identified by 2x and 3x rev. components. The 1x rev. component identifies the crack in a beam element close to the actual one (element 24 instead of 23) with an error of 1.7% with respect to the overall length of the rotor. The crack depth is identified using only the value of the 2x rev. equivalent bending moment M_2 , which is equal to 301 Nm. The static bending moment M is equal to 548 Nm in element 23 (figure 7). The shaft diameter D is 70 mm and element 23 length l is 53.5 mm, so that r.h.s. of eq. (41) is 0.425 that corresponds in figure 5 to a depth of 47%.

Moreover, the 1x rev. component identifies the position with a particularly reduced value of the relative residual. This result has been obtained by processing the experimental data in the following way: first the unbalances on the disks were identified, and then the dynamical behavior due to the unbalances only has been subtracted from measured data in order to obtain the bow induced vibrations. This leads to a very good agreement between the experimental and the simulated behavior for the 1x rev. component as shown in figure 38 and figure 39, in which bow and unbalances have been superimposed. Due to this procedure, it was considered not pertinent to use M_1 to identify the crack depth.

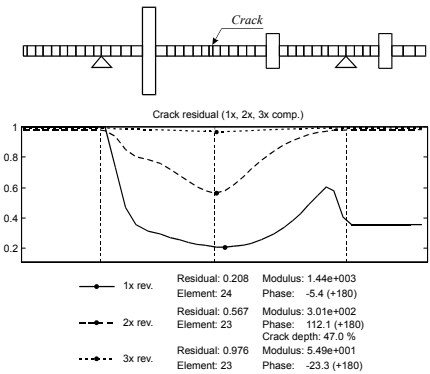


Figure 37. 47% cracked shaft. Relative residuals of the crack identification.

In regards to the 2x rev. component, the relative residual can be considered as good, but the most remarkable result is the exact identification of the depth of the crack. Also the simulated behavior in figure 40 and figure 41 is good.

As concerning the 3x rev. component, the relative residual is quite high, but this can be explained by considering that this component is normally masked by noise. This notwithstanding, if M_3 were deemed useful to identify the crack depth, it resulted equal to 54.9 Nm that made r.h.s. of eq. (41) to be equal to 0.077 that corresponds in figure 5 to a depth of 30%. However, the residual curve presents a well defined minimum in correspondence of the crack even this is not so evident in figure 37 due to the scale. The comparison is reported in figure 42 and figure 43 for this component.

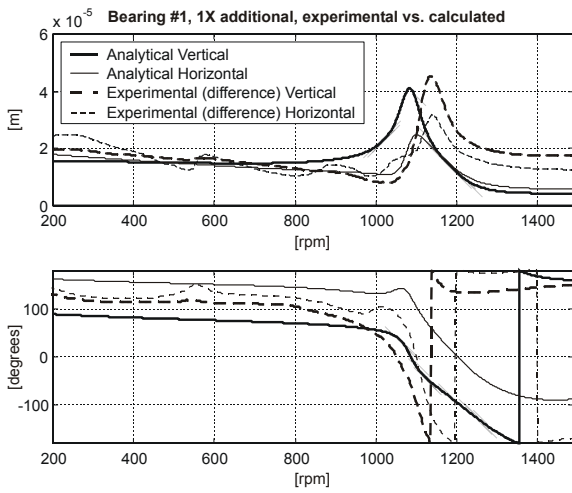


Figure 38. Case 3, crack: comparison between simulated and experimental 1x rev. vibration components for bearing 1.

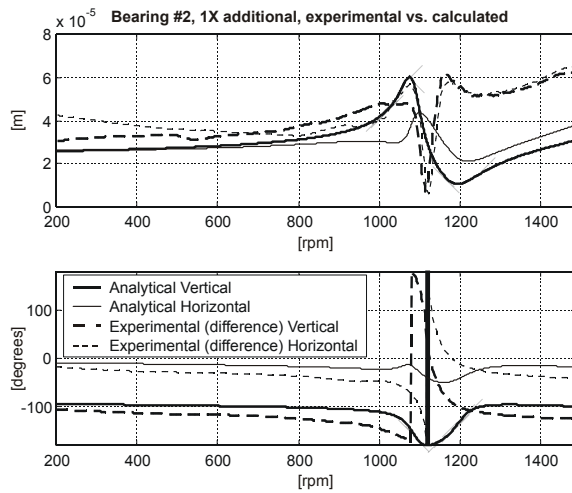


Figure 39. Case 3, crack: comparison between simulated and experimental 1x rev. vibration components for bearing 2.

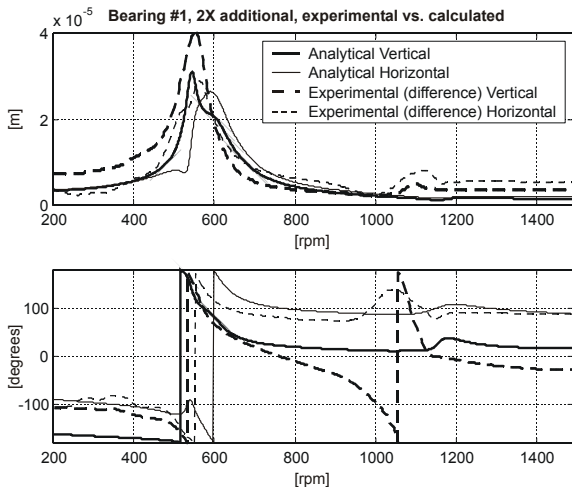


Figure 40. Case 3, crack: comparison between simulated and experimental 2x rev. vibration components for bearing 1.

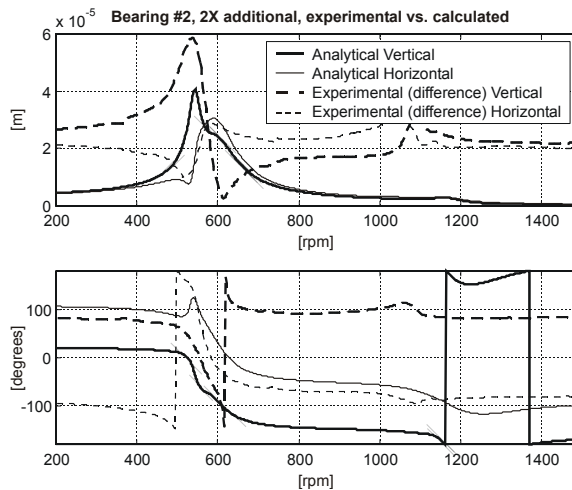


Figure 41. Case 3, crack: comparison between simulated and experimental 2x rev. vibration components for bearing 2.

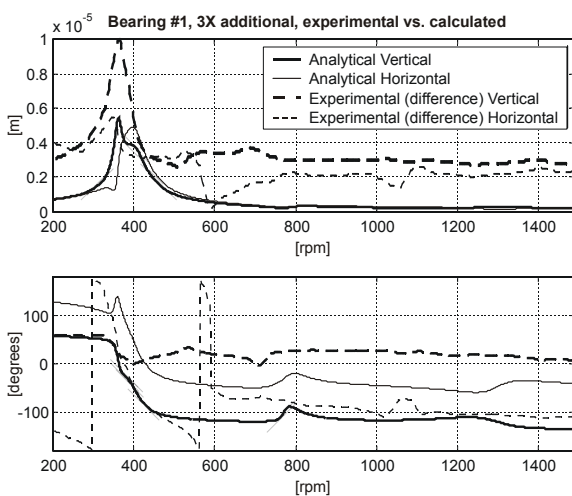


Figure 42. Case 3, crack: comparison between simulated and experimental

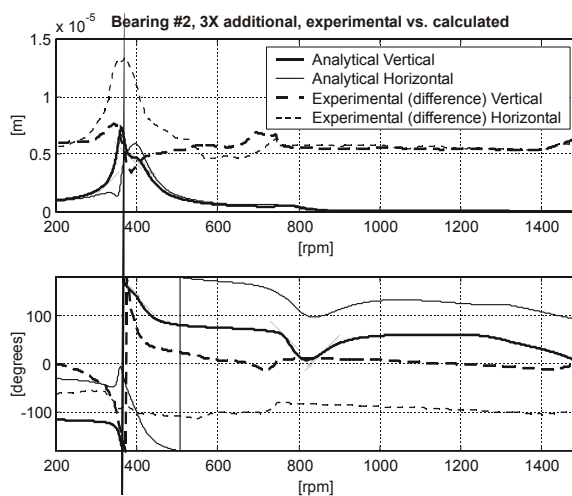


Figure 43. Case 3, crack: comparison between simulated and experimental

5 CONCLUSIONS

A model based transverse crack identification procedure in the frequency domain has been presented and applied to experimental results obtained on a medium size test rig. Three cases of crack identifications have been presented and the results, which are rather accurate, confirm the validity of the proposed approach. Since only measurements in the bearings, or close to the bearings, are used, the method is suitable for field applications, because these measuring planes are standard in industrial machines.

6 ACKNOWLEDGMENTS

The authors wish to thank Division Recherche et Développement, Dép. Acoustique et Mécanique Vibratoire of EDF - Electricité de France for having provided test rig data.

REFERENCES

- [1] Schmerling J.M. and Hammon J.C., "Investigation of the Tennessee Valley Authority Gallatin Unit No. 2 turbine rotor burst", American Power Conference, Chicago, Apr. 1966.
- [2] Jack A.R and Patterson A.N., "Cracking in 500 MW LP rotor shafts", 1st Mechanical Engineering Conference, 1976.
- [3] Haas G., "Großschäden durch Turbinen- oder Generatorläufer, entstanden im Bereich bis zur Schleuderdrehzahl", Maschinenschaden, 50, 1977, 195-204.
- [4] Greco J., Agnew J.R., Erhardt K., Bertilsson J.E. and Stys Z.S., "Cumberland steam plant-cracked IP rotor coupling", American Power Conference, Chicago, 1978.
- [5] Nilsson L.R.K., On the Vibration Behaviour of a Cracked Rotor, IFToMM Intl. Conf. Rotordynamic Problems in Power Plants, Sept.-Oct. 1982, Rome, Italy, pp. 515-524.
- [6] ALLIANZ Berichte, nr. 24 Nov. 1987, ISSN 0569-0692.
- [7] Imam I., Azzaro S.H., Bankert R.J. and Scheibel J., "Development of an On-Line Rotor Crack Detection and Monitoring System", ASME Journal of Vibration, Acoustics, Stress and Reliability in Design (1989) 111(3), 241-250.
- [8] Bach H. and Markert R., "Determination of the fault position in rotors for the example of a transverse crack", in: Fu-Kuo Chang, (Ed.), Structural Health Monitoring, Technomic Publ. Lancaster/Basel, 1997, pp. 325-335.
- [9] Sekhar A.S., "Crack identification in a rotor system: A model-based approach", Journal of Sound and Vibration (2004) 270(4-5), 887-902.
- [10] Dilella M. and Morassi A., "The use of antiresonances for crack detection in beams" Journal of Sound and Vibration (2004) 276(1-2), 195-214.
- [11] Gounaris G.D. and Papadopoulos C.A., "Crack identification in rotating shafts by coupled response measurements", Engineering Fracture Mechanics, (2002) 69(3), 339-352
- [12] Dong G.M., Chen J. and Zou J., "Parameter identification of a rotor with an open crack", European Journal of Mechanics A/Solids (2004) 23(2), 325-333.
- [13] Seibold S. and Winert K., "A time domain method for the localization of cracks in rotors", Journal of Sound and Vibration (1996) 195(1), 57-73.
- [14] Bucher I. and Seibold S., "A Two-stage approach for enhanced diagnosis of rotating machines", IFToMM 5th International Conference on Rotor Dynamics, Darmstadt, Sept.

- 1998, 338-349.
- [15] Wauer J., "On the dynamics of cracked rotors: A literature survey", *Applied Mechanics Review* (1990) 43(1), 13-18.
 - [16] Gasch R., "A Survey of the Dynamic Behaviour of a Simple Rotating Shaft with a Transverse Crack", *Journal of Sound and Vibration* (1993) 160(2), 313-332.
 - [17] Dimarogonas A.D., "Vibration of Cracked Structures. A State of the Art Review", *Engineering Fracture Mechanics* (1996) 55(5), 831-857.
 - [18] Diana G., Bachschmid N. and Angeli F., "An on-line crack detection method for turbogenerators", *IFTOMM-JSME Int. Conf. on Rotordynamics*, September 1986, Tokyo, 385-390
 - [19] Bachschmid N., Pennacchi P., Tanzi E. and Vania A., "Identification of Transverse Crack Position and Depth in Rotor Systems", *Meccanica* (2000) 35(6), 563-582.
 - [20] Bachschmid N., Vania A. and Audebert S., "A Comparison of Different Methods for Transverse Crack Modelling in Rotor Systems", *ISROMAC-8 Conference*, March 2000, Honolulu, Hawaii, 1057-1064.
 - [21] Bachschmid N., Pennacchi P. and Vania A., "Identification of Multiple Faults in Rotor Systems", *Journal of Sound and Vibration* (2002) 254(2), 327-366.
 - [22] Bachschmid N., Pennacchi P., Vania A., Zanetta G.A. and Gregori L., "Use of modal representation for the supporting structure in model based fault identification of large rotating machinery: part 1 – theoretical remarks", in press on *Mechanical Systems and Signal Processing*, available online on ScienceDirect.
 - [23] Vania A. and Pennacchi P., "Experimental and Theoretical Application of Fault Identification Measures of Accuracy in Rotating Machine Diagnostics", *Mechanical Systems and Signal Processing*, Vol. 18, No. 2, 2004, ISSN 0888-3270, pp.329-352.
 - [24] Bachschmid N., Pennacchi P., Tanzi E. and Audebert S., "Transverse Crack Modeling and Validation in Rotor Systems, Including Thermal Effects", *International Journal of Rotating Machinery* (2003) 9(2), 113-126.